Formulation and Evaluation of Nano-emulsion for Intranasal Nose-to-Brain Delivery: A Promising Strategy for Alzheimer's Disease Management

Anirudha Munde[1]*, Dr. Vishakha Chauhan[2], Dr. Sudha Vengurlekar[3], Dr. Sachin Kumar Jain[4]

[1]Research Scholar, Department of Pharmacy, Oriental University, Indore (M.P)
[2]Associate Professor, Department of Pharmacy, Oriental University Indore. (M.P)
[3]Dean, Department of Pharmacy, Oriental University Indore. (M.P)
[4]HOD, Department of Pharmacy, Oriental University Indore. (M.P)
***Corresponding author*:**
Anirudha V. Munde
Research Scholar, Department of Pharmacy, Oriental University, Indore (M.P)
anirudhamunde@gmail.com

Abstract: Rivastigmine HCl (RHC) is commonly prescribed to manage mild to moderate dementia, including cognitive decline associated with Alzheimer's and Parkinson's diseases. While it does not halt disease progression, it has been shown to enhance cognitive function in some patients. This study focused on developing an RHC nanoemulsion (RHC-NE) using the Pseudoternary phase diagram method, which aids in optimizing formulation based on the solubility of RHC in surfactants and cosurfactants. The final formulation of RHC-NE consisted of 3.7% ethyl oleate as the oil phase, 11.5% surfactant (a 1:1 mixture of polyethylene glycol ester of 15-hydroxystearic acid and polyoxyethylene 35 castor oil), 3% polyethylene glycol 400 as the cosurfactant, and 82% aqueous phase. Pharmacokinetic analysis revealed that the brain-targeting efficiency of RHC was higher when administered nasally compared to the intravenous route.

Keywords: Rivastigmine, Alzheimer's disease, Nano-emulsion, Nose to Brain, Drug delivery, etc.
How to cite this article: Munde A, Chauhan V, Vengurlekar S, Jain SK. Formulation and evaluation of nano-emulsion for intranasal nose-to-brain delivery: a promising strategy for Alzheimer's disease management. Int J Drug Deliv Technol. 2026;16(75s): 85-94. DOI: 10.25258/ijddt.16.75s.9

Introduction

Alzheimer's disease (AD) is a progressive neurodegenerative disorder that affects millions worldwide, with an estimated 47 million people living with the condition according to the World Alzheimer Report (2016). AD leads to the death of brain cells, resulting in memory loss and a gradual decline in cognitive functions [1-3]. In the brain, cholinergic neurons release acetylcholine (ACh), a neurotransmitter essential for short-term memory formation and cognitive processing at the biochemical level [2, 4]. ACh is broken down into acetyl and choline by the enzymes acetylcholinesterase (AChE) and butyrylcholinesterase (BuChE), leading to impaired neurotransmission. To counteract this, cholinesterase inhibitors like Rivastigmine, donepezil, galantamine, and tacrine are commonly used in AD treatment, as they block AChE activity, preserving ACh levels and improving central cholinergic function. However, these drugs only target AChE and do not inhibit BuChE, which continues to contribute to ACh breakdown, presenting an ongoing challenge in AD therapy [2, 5].

Among the various cholinesterase inhibitors, Rivastigmine hydrochloride (RHC) stands out as the only drug that inhibits both acetylcholinesterase (AChE) and butyrylcholinesterase (BuChE), effectively preventing the hydrolysis of acetylcholine by both enzymes. As a result, RHC was chosen as the primary drug for this study. RHC is a derivative of phenyl carbamate and undergoes significant first-pass metabolism when taken orally, leading to an absolute bioavailability of only 36% after a 3 mg dose [2, 5, and 6]. Due to its hydrophilic nature, RHC has limited penetration into the brain after oral administration, requiring frequent dosing. This can result in pronounced cholinergic side effects such as bradycardia, nausea, dyspepsia, vomiting, and anorexia [3, 5, and 6].

The noninvasive intranasal route for delivering drugs to the brain is gaining considerable attention among various strategies for brain drug delivery. One of the primary benefits of this approach is the direct connection between the nasal cavity and the central nervous system (CNS), enabling the drug to bypass the blood-brain barrier (BBB). This results in increased drug concentrations in the brain while minimizing systemic side effects by reducing the drug's exposure to other parts of the body. The nasal mucosa's neural pathways, particularly through the olfactory and trigeminal nerves, provide a direct route

to the brain, allowing drugs to reach the olfactory bulb and brainstem, from where they are distributed throughout the CNS [7].

However, there are certain limitations associated with the intranasal delivery route, including a restricted volume of drug formulations (typically between 25–200 µL) that can be effectively administered. Additionally, this route is subject to rapid mucociliary clearance and limited permeability of nasally applied drugs. Despite these challenges, the use of chemical penetration enhancers and advanced drug delivery systems, such as nanoemulsions, liposomes, and nanoparticles, has shown promise in overcoming these obstacles [8].

Microemulsions are considered thermodynamically stable, in contrast to nanoemulsions (NE), which are kinetically stable. From a formulation perspective, a higher surfactant-to-oil ratio (SOR) is necessary for creating a microemulsion compared to a nanoemulsion. As a result, microemulsions tend to have smaller particle sizes than nanoemulsions. In microemulsions, the particle size distribution typically shows a single, narrow peak, while nanoemulsions can exhibit either a single or multiple peaks, which may vary in width. The particles in nanoemulsions are generally spherical, whereas microemulsions can present both spherical and non-spherical shapes. Additionally, microemulsions are less stable than nanoemulsions when subjected to dilution or temperature fluctuations. Dilution of microemulsions typically results in a decrease in globule size, while nanoemulsions maintain stable globule size under the same conditions. Temperature variations do not significantly affect the structure or droplet size of nanoemulsions, but they do impact the stability and size of droplets in microemulsions [9].

Nanoemulsions offer several advantages, including simplicity in preparation, the use of biocompatible excipients, and enhanced properties due to their smaller globule size (less than 200 nm). These advantages contribute to increased solubility, dissolution rates, and encapsulation efficiency, as well as their ability to easily permeate the olfactory mucosa and reach the brain. This results in efficient absorption of oil droplets [8, 10, 11]. Due to the presence of both lipophilic and hydrophilic domains, nanoemulsions are highly effective for incorporating a wide range of both hydrophilic and hydrophobic drugs [2]. Furthermore, the encapsulation of drugs within the oil phase ensures nanoemulsions exhibit high stability, protecting drugs from hydrolysis and enzymatic degradation under physiological conditions [11]. Based on these findings, the current study aims to develop a nanoemulsion of RHC that enhances brain delivery via the nasal route. This approach aims to bypass first-pass metabolism, prevent distribution to non-targeted sites, and ultimately improve brain bioavailability, reduce the need for frequent dosing, and minimize peripheral side effects.

Material and Method

Rivastigmine hydrochloride (RHC) was received as a kind gift sample from Torrent Pharmaceuticals Ltd. (Himachal Pradesh, India).

Method

Determination of Solubility and Lipid-Water Partition Coefficient of RHC

Various oils, emulsifiers, and co-emulsifiers were selected as solvents to evaluate the saturated solubility of RHC. To conduct this, RHC powders were added to 0.5 mL of different oils (such as ethyl oleate and isopropyl myristate), surfactants (including polyethylene glycol ester of 15-hydroxystearic acid (HS-15), polyoxyethylene 35 castor oil (EL-35), Tween-80, and a blend of HS-15 and EL-35 in a 1:1 ratio), and cosurfactants (such as polyethylene glycol 400 (PEG400), 1,2-propanediol, and absolute ethanol). The mixture was stirred using a magnetic stirrer for 30 minutes, followed by shaking at 37°C for 48 hours. Afterward, it was centrifuged at 12,000 r/min for 15 minutes. The supernatant obtained was diluted with methanol, and RHC concentration was analyses using high-performance liquid chromatography (HPLC). The HPLC system included a Shimadzu LC-10AT solvent delivery pump (Shimadzu, Kyoto, Japan) with a 20 µL loop and a UV-visible detector. A Welchrom C18 analytical column (4.6 × 200 nm, 5 µm) was used for the analysis. The eluate was observed at a wavelength of 220 nm. The mobile phase consisted of methanol and water in an 80:20 (v/v) ratio, flowing at a rate of 1.0 mL/min under ambient conditions. The lipid-water partition coefficient of RHC was determined using an octanol/water extraction method, followed by HPLC analysis. In this process, 40 mg of RHC powder was dissolved in 2 mL of octanol pre-saturated with distilled water inside 5 mL polypropylene centrifuge tubes. Subsequently, 2 mL of distilled water pre-saturated with octanol was added to each tube. The tubes were then vigorously mixed for 15 minutes and shaken for 72 hours at 37°C to achieve equilibrium. After centrifugation, RHC concentrations in both the octanol and water phases were measured. The lipid-water partition coefficient (log P) was then calculated using the following equation:

$$\log P = \log \frac{C_{oil} \times V_{oil}}{C_{water} \times V_{water}}$$

Construction of Pseudo ternary Phase Diagram

Pseudo-ternary phase diagrams were developed using the aqueous titration method. The ratios of the combined surfactant to cosurfactant (Km values) were adjusted to 1:1, 2:1, 3:1, and 4:1. At each Km value, the weight ratios of oil to the surfactant mixture varied as follows: 1:9, 2:8, 3:7, 4:6, 5:5, 6:4, 7:3, 8:2, and 9:1. After thoroughly mixing the oil with the emulsifier blend, the mixture was titrated with distilled water under moderate stirring. The amount of water required to form transparent or translucent nanoemulsions was recorded. The pseudo-ternary phase diagrams were then constructed based on the proportion of each component. The final composition of RHC-NE consisted of 3.6% ethyl oleate as the oil phase, 11.4% surfactant (HS-15 and EL-35 in a 1:1 ratio), 3% PEG 400 as a cosurfactant, and 82% aqueous phase.

Physicochemical Characterization of RHC-NE

Physical stability determination

RHC-NE was subjected to centrifugation at 15,000 r/min for 15 minutes. Afterward, observations were made to determine whether it exhibited precipitation, phase separation, or turbidity.

Particle size measurement

The zeta potential and particle size were measured using a Malvern Nano series particle size analyzer (Malvern, UK), with data analysis conducted through the Malvern Zetasizer software (Malvern, UK).

Type identification

The classification of the nanoemulsion was identified using the oil-soluble dye Sudan Red III (red) and the water-soluble dye methylene blue (blue). The movement of both dyes within the nanoemulsion was monitored to analyze their diffusion rate.

Morphological analysis

A drop of RHC-NE was placed onto a carbon-coated copper grid and stained with 1% phosphotungstic acid. After allowing it to dry, the morphology of the RHC-NE was examined using a JEM-1200EX transmission electron microscope (JEOL, Tokyo, Japan).

Stability of RHC-NE

The formulated RHC-NE was stored at 25°C for 25 days. Its particle size, polydispersity index (PDI), and zeta potential were analyzed at intervals of 0, 5, 10, 15, 20, and 25 days.

Sterilization of RHC-NE

To identify an appropriate sterilization method, RHC-NE was subjected to three different techniques: high-temperature autoclaving, ultraviolet (UV) irradiation, and filtration through a microporous membrane. After sterilization, the stability of both RHC-NE and the bacteria within RHC was evaluated.

In-Vitro Drug Release Test

The release test for RHC-NE was conducted using the ZRS-8G intelligent dissolution testing apparatus. A dialysis bag with a molecular weight cutoff of 8,000–14,000 was used to contain the RHC-NE or RHC suspension, equivalent to 4 mg of RHC. The experiment was carried out in 200 mL of Simulated Nasal Electrolyte Solution (SNES) with 1% Tween-80, maintained at 37 ± 0.5°C and stirred at 100 r/min. The SNES (pH 5.5) was prepared using 7.45 mg/mL NaCl, 1.29 mg/mL KCl, and 0.32 mg/mL $CaCl_2 \cdot 2H_2O$. At predetermined intervals (0.25, 0.5, 1, 2, 4, 6, 8, 10, 12, 24, 36, 48, 60, and 72 hours), 0.5 mL of the dissolution medium was sampled and replaced with an equal volume of fresh isothermal SNES. Before HPLC analysis, all samples were filtered using a 0.22 μm Millipore filter.

Pharmacokinetic Study

All animal experiments in this study were conducted with the approval of the Institutional Animal Ethics Committee at Shandong First Medical University and Shandong Academy of Medical Sciences. Kunming mice, weighing approximately 20 ± 2 g, were obtained from China Biologic Products Holdings, Inc. The mice were provided with a standard diet and had unrestricted access to distilled water. Following an overnight fasting period, the mice were randomly assigned to two groups. One group received an intravenous (IV) dose of RHC-NE at 40 mg/kg, while the other group received an intranasal (IN) dose of RHC-NE at 10 mg/kg. Blood samples were collected from the orbital vein at various time points: 5, 15, 30, 60, 120, 180, 240, and 360 minutes post-administration. After sample collection, the mice were euthanized and perfused transcardially with normal saline. Brain tissues were then extracted and homogenized in saline. The blood samples were subjected to centrifugation at 3000 r/min for 10 minutes. Subsequently, 100 μL of plasma or brain tissue homogenate was mixed with 300 μL of acetonitrile in a centrifuge tube. After vortexing for 5 minutes, the mixture was centrifuged at 10000 r/min for another 10 minutes, and the resulting supernatant was collected. To further purify the samples, NaCl was added, followed by another centrifugation at 10000 r/min for 10 minutes. The RHC concentrations in plasma and brain tissues were analyzed using high-performance liquid chromatography (HPLC)

at a wavelength of 220 nm. Pharmacokinetic parameters for both administration routes were determined using DAS 2.2.1 software (DAS Studio, Shanghai, China). To assess brain targeting efficiency after intranasal administration, drug-targeting efficiency (DTE %) and drug-targeting percentage (DTP %) were calculated using specific formulas.

$$DTE\ \% = \frac{[AUC\ brain / AUC\ blood]\ i.n.}{[AUC\ brain / AUC\ blood]\ i.v.} \times 100$$

$$DTP\ \% = \frac{[Bi.n. - Bx]}{[Bi.n.]} \times 100$$

$$Bx = \frac{[B\ i.v.]}{[B\ i.v.]} \times P\ i.n.$$

Where Pi:v: , Bi:v: , Pi:n: , and Bi:n: denote the area under the curve (AUC) from time zero to time t (AUC0−t) of RHC-NE in plasma (P) and brain (B) tissue that were obtained after IV and IN administration, respectively. Bx represents the brain AUC fraction contributed by systemic circulation through the blood-brain barrier (BBB) after IN administration.

Cell Culture and Treatments

The SH-SY5Y human neuroblastoma cell line was acquired for this study. The cells were cultured in high-glucose Dulbecco's modified Eagle's medium (Hyclone, Logan, UT, USA), supplemented with 10% fetal bovine serum and 100 U/mL penicillin, along with 100 µg/mL streptomycin (Gibco, USA). The cells were maintained at 37°C in a 5% CO2 humidified incubator. To assess the effect of L-glutamate (L-Glu) in inducing excitotoxicity, SH-SY5Y cells were exposed to various concentrations of L-Glu (5, 10, 15, 20, 25, 30, 35, and 40 mmol/L) for different time points (4, 6, 8, 10, and 12 hours). Cell viability was determined using the MTT assay. The conditions of 30 mmol/L L-Glu for 6 hours were selected to establish the L-Glu-induced SH-SY5Y cell model. Subsequently, the influence of the blank nanoemulsion on L-Glu-induced SH-SY5Y cells was examined. SH-SY5Y cells were seeded in 96-well plates (2 × 10^4 cells/well) and cultured for 24 hours. The cells were treated with either a blank medium (model group) or a blank nanoemulsion in medium (drug-free NE group, at concentrations of 10 µmol/L and 0.1 µmol/L) for 6 hours, followed by exposure to 30 mmol/L L-Glu for an additional 6 hours. The control group was maintained in blank medium only. Cell viability was assessed using the MTT assay. Subsequently, the effects of RHC-NE on L-Glu-induced SH-SY5Y cells were evaluated. SH-SY5Y cells were plated in 96-well culture plates at a density of 2 × 10^4 cells per well (100 µL per well). After 24 hours of incubation, cells were treated with blank nanoemulsion (model), RHC-NE at 10 µmol/L or 0.1 µmol/L, and incubated for 6 hours. The culture medium was then replaced with 30 mmol/L L-Glu and incubated for another 6 hours. The control group was treated with blank nanoemulsion for 6 hours and then with blank medium for the following 6 hours. Cell viability was measured using the MTT assay.

Cell Viability Assay

The MTT assay was performed following established protocols. After applying the respective treatments, 20 µL of MTT solution (5 mg/mL) was added to each well, and the plate was incubated at 37°C for 4 hours. After incubation, the supernatant was removed, and 150 µL of dimethyl sulfoxide was added to dissolve the formazan crystals. The optical density (OD) was then measured using a microplate reader at 570 nm. Cell viability for each treatment group was calculated by comparing the OD values.

Cell viability = (%) = OD experiment/OD control 100

Terminal Deoxynucleotidyl Transferase- (TdT-) Mediated Deoxyuride-Triphosphate- (dUTP-) Biotin NickEnd Labelling (TUNEL) Staining

Apoptotic cells were identified using the In Situ Cell Death Detection Kit (Roche), which employs TUNEL technology. Following treatment with RHC-NE/L-Glu, SH-SY5Y cells were fixed with 4% paraformaldehyde for 10 minutes and permeabilized with 0.1% Triton X100 for 1 minute at room temperature. The cells were then exposed to a mixture of TdT and dUTP, followed by incubation for 2 hours at 37°C. After three washes with phosphate-buffered saline, the cells were stained with 4, 6-diamino-2-phenylindole (DAPI) for 10 minutes at room temperature. Images were captured using a fluorescence microscope.

Statistical Analysis

The data are expressed as the mean ± standard deviation (SD). Statistical analysis was conducted using GraphPad Prism 6 software. Comparisons were made using one-way analysis of variance (ANOVA), with a P value of less than 0.05 considered statistically significant.

Result and Discussion

Solubilities of RHC in Different Surfactants and Cosurfactants

Figure 1 illustrates the solubility of RHC in various surfactants and cosurfactants. Among the oils tested, RHC demonstrated the highest solubility in ethyl oleate (38.04 ± 1.3 mg/mL), followed by isopropyl myristate (28.2 ±

0.2 mg/mL). Compared to oils, surfactants significantly enhanced RHC solubility, with values recorded as 181.7 ± 1.2 mg/mL in HS-15, 158.40 ± 7.7 mg/mL in EL-35, 172.89 ± 8.2 mg/mL in Tween 80, and 170.70 ± 8.2 mg/mL in a combination of HS-15 and EL-35. For cosurfactants, the solubility levels were measured at 122.9 ± 8.8 mg/mL in PEG400, 72.2 ± 5.9 mg/mL in absolute ethanol, and 9.9 ± 0.8 mg/mL in 1, 2-propanediol.

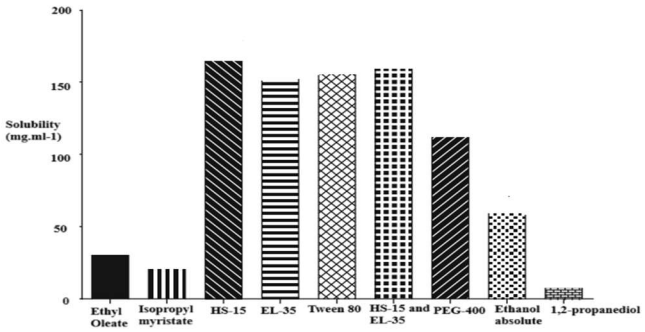

Fig. 1: Solubility of RHC in different surfactants and cosurfactants

Lipid-Water Partition Coefficient of RHC

The concentrations of the two phases, measured using HPLC, were found to be 2.5 mg/mL in oil and 1.5 µg/mL in water. Using equation (1), the calculated log P value was 3.24

Pseudoternary Phase Diagrams

The Pseudoternary phase diagrams for various surfactants are presented in Figure 2. The largest shaded region was observed when the surfactant comprised a 1:1 mixture of HS-15 and EL-35, with a Km ratio of 4:1 (Figure 2(c)).

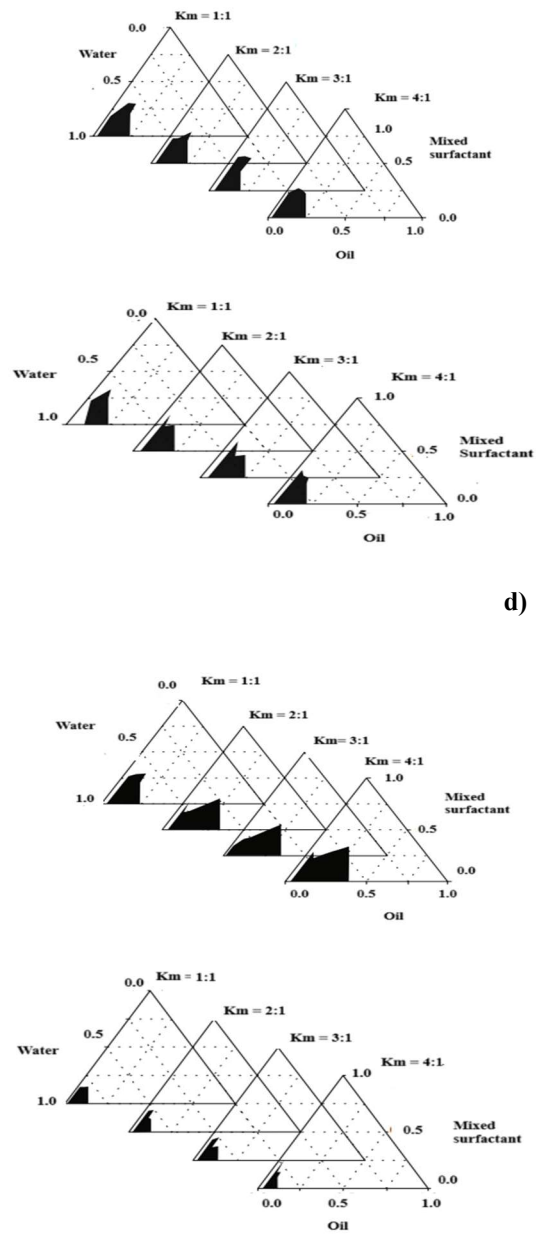

Fig. 2: Pseudoternary phase diagrams of the oil-surfactant-water systems. The shaded region represents nanoemulsion. (a) EL-35 as surfactant; (b) HS-15 as surfactant; (c) a mixture of EL-35 and HS-15 at a ratio of 1 : 1 as surfactant; (d) Tween-80 as surfactant.

Characteristics of RHC-NE

The stability assessment revealed that the RHC-NE appeared as a clear, transparent, and slightly blue-opalescent liquid with a faint odor before undergoing high-speed centrifugation. Following centrifugation, it remained a light blue transparent liquid without any signs of phase separation, turbidity, or precipitation. The

average particle size was measured at 23.34 ± 0.48 nm, with a PDI of 0.116 ± 0.058 (Figure 3(a)), indicating a small and uniform particle distribution. The zeta potential of RHC-NE was recorded at −9.89 ± 0.65 mV (Figure 3(b)). A type identification test demonstrated that the diffusion rate of the water-soluble dye methylene blue was greater than that of the oil-soluble dye Sudan Red III (Figure 3(c)). Morphological analysis confirmed that the RHC-NE particles were spherical, evenly sized, and well-dispersed (Figure 3(d)).

a) **b)**

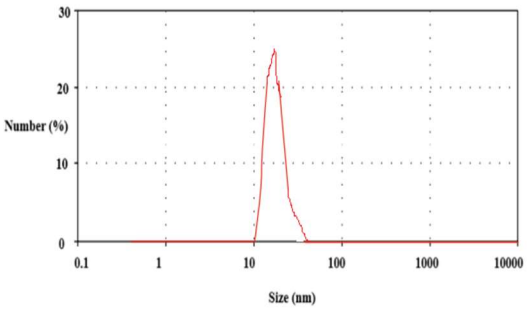

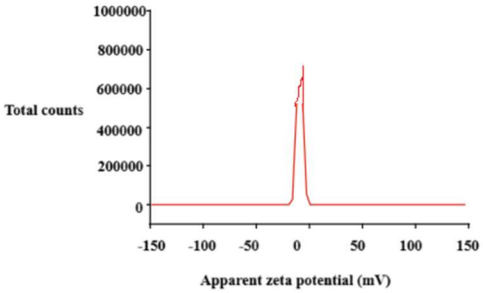

c) **d)**

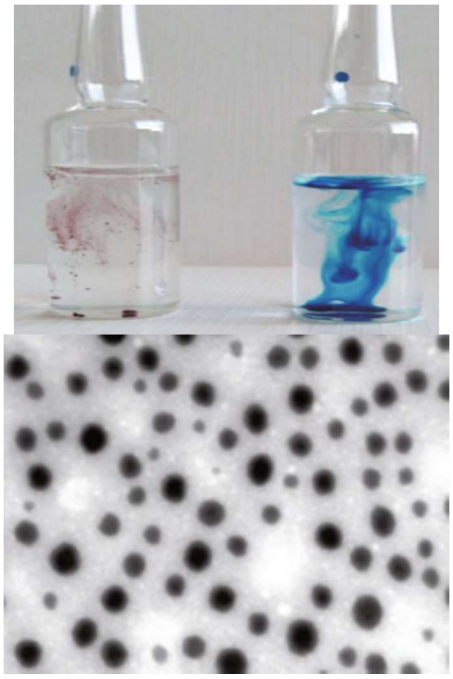

Fig. 3: Characteristics of RHC-NE. (a) Particle size of RHC-NE. (b) Zeta potential of RHC-NE. (c) The different diffusion velocity of oil dye Sudan Red III (left) and water-soluble dye methylene blue (right) in the RHC-NE. (d) TEM images of RHC-NE

Stability of RHC-NE

Table 1 demonstrates that the particle size, PDI, and zeta potential of the RHC-NE exhibited minimal variation over the storage period, suggesting strong thermodynamic stability of the prepared RHC-NE.

Table 1: Average particle size, PDI, and absolute zeta potential of RHC-NE during storage

Time (days)	Particle size (nm)	PDI	Zeta (mv)
0	22:08 ± 0:07	0:054 ± 0:014	−7:25 ± 1:86
5	22:23 ± 0:24	0:069 ± 0:015	−6:46 ± 1:91
10	22:62 ± 0:43	0:146 ± 0:033	−8:70 ± 2:13
15	22:13 ± 0:12	0:082 ± 0:007	−6:31 ± 3:67
20	21:97 ± 0:24	0:064 ± 0:003	−4:05 ± 1:11
25	22:16 ± 0:28	0:136 ± 0:015	−4:81 ± 1:06

In-Vitro Release

The dialysis bag contained 4 mg of RHC-NE, which was released into 200 mL of SNES medium. Over 72 hours, RHC release followed a time-dependent pattern, with RHC-NE exhibiting a higher release rate than RHC suspensions. By the end of the 72-hour period, RHC-NE had released approximately 80% of its drug content, whereas the RHC suspension had only released around 40% (Figure 4). This suggests that RHC-NE has a relatively high release rate in biological conditions. To analyze the correlation between cumulative RHC release and time, kinetic modeling was applied. Table 2 presents the model fitting results for the in vitro release profile of RHC. The most suitable mathematical model was determined based on the correlation coefficient (r) of the equation. The in vitro release of RHC-NE in SNES with 1% Tween-80 followed a first-order kinetic model, while the RHC suspension adhered to the Higuchi model.

Table 2: Model fitting for in vitro release profile of RHC

Model	Osthole nanoemulsion	r	Osthole suspension	r
Zero-order	Q = 1:2206t + 5:1463	0.9832	Q = 0:6086t + 3:3969	0.9805
First-order	Ln (100−Q) = −0:0248t + 4:6189	0.9979	Ln (100−Q) = −0:0080t + 4:5778	0.9905
Higuchi	Q= 12:085t 1/2 − 11:956	0.9929	Q = 5:545t 1/2 − 4:6975	0.9934

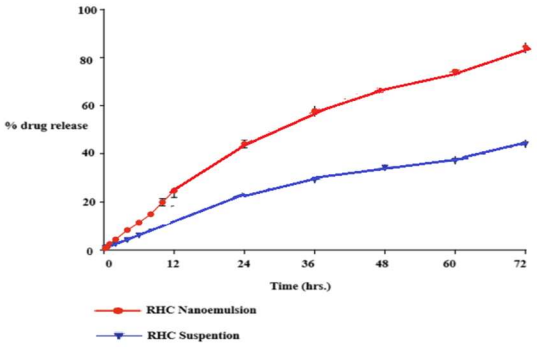

Fig. 4: In vitro release of RHC from nanoemulsion compared with suspension

Pharmacokinetic Profile

In plasma, the RHC concentration reached the maximum just 5 minutes after administration by the IV route, whereas it took 30 minutes to reach the maximum concentration by the IN route (Figure 5). Moreover, the maximum concentration of RHC in plasma by the IN route (4:54 ± 0:68 µg/mL) was lower than that by the IV route (10:64 ± 1:45 µg/mL). For AUC0−t and AUC0−∞, there was no significant difference between IV and IN administration. The clearance rate by the IV route was 1.80 times higher than that of IN administration (Table 3). In the brain, the maximum concentration of RHC by IN (34:05 ± 2:57 µg/mL, 5 minutes after administration) was higher than that by IV (26:63 ± 1:87 µg/mL, 30 minutes after administration) (Figure 5 and Table 3). The AUC0−t and AUC0−∞ of RHC by IN were 0.62 times and 0.64 times higher than that of IV administration, respectively. The clearance rate by IV was 7.09 times higher than that of IN administration (Table 4). The AUC brain/ AUC plasma values after IV and IN administrations of RHC-NE were 2.83 and 4.89, respectively. The DTE% and DTP% of RHC-NE after IN administration were 208.28 % and 52.81 %, respectively.

a) **b)**

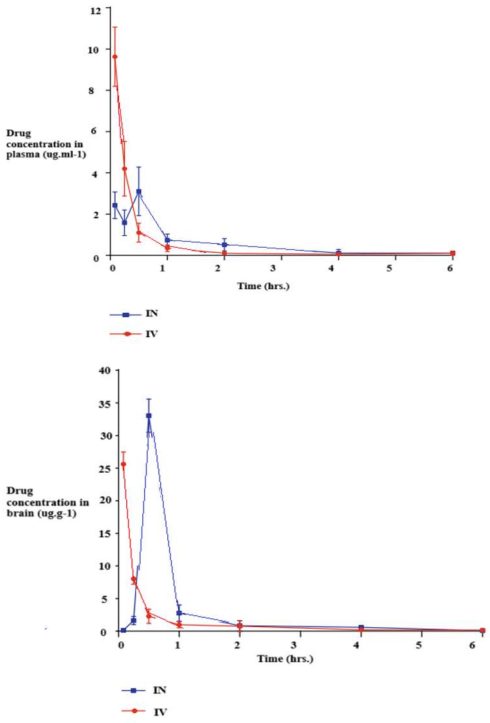

Fig. 5: Pharmacokinetics curve of RHC-NE in plasma and brain tissue after IN and IV administrations: (a) drug concentration in plasma; (b) drug concentration in the brain

Table 3: Pharmacokinetic parameters of RHC-NE in plasma after IN and IV administrations

Parameters	C max (µg/mL)	AUC 0−t (µg/Ml □h)	AUC0 −∞ (µg/mL □h)	CL (l/H/kg)	MRT 0−t (h)
Intranasal	4:54 ± 0:68	3:91 ± 0:19	3:94 ± 0:23	3:87 ± 1:05	2:24 ± 0:31
Intravenous	10:64 ± 1:44	4:71 ± 0:52	4:75 ± 0:54	8:98 ± 0:70	1:53 ± 0:23

Table 4: Pharmacokinetic parameters of RHC-NE in the brain after IN and IV administrations

Parameters	C max (µg/mL)	AUC 0−t (µg/Ml □h)	AUC0 −∞ (µg/mL □h)	CL (l/H/kg)	MRT 0−t (h)
Intranasal	34:05 ± 3:57	17:88 ± 2:36	18:56 ± 2:49	0:37 ± 0:24	0:83 ± 0:15
Intravenous	26:63 ± 1:87	11:46 ± 2:70	11:81 ± 2:73	2:92 ± 0:55	0:48 ± 0:25

Sterilization Method of RHC-NE

The RHC-NE was structured following high-temperature autoclaving (Figure 6(c)). After two hours of UV exposure, bacteria were still present in the RHC-NE, whereas no bacterial contamination was observed when a microporous membrane was used for sterilization. Consequently, the microporous membrane was chosen for filtering the RHC-NE.

a) **b)** **c)**

Fig. 6: Influence of three different sterilization methods on the stability of RHC-NE: (a) microporous filter; (b) UV sterilization; (c) autoclave

RHC-NE Protects SH-SY5Y Cells against L-Glu-Induced Apoptosis

TUNEL staining identifies DNA damage by marking free 3′-hydroxyl ends, which emerge during both early and late stages of apoptosis due to genomic DNA fragmentation. As a widely used method to assess apoptosis, TUNEL staining specifically highlights apoptotic cells. Figure 7 illustrates that L-Glu treatment notably increased the number of TUNEL-positive cells (red fluorescence-labeled), compared to the control SH-SY5Y cells, suggesting that L-Glu (30 mmol/L) induced apoptosis in SH-SY5Y cells. However, pretreatment with RHC-NE reduced the number of TUNEL-positive cells relative to the L-Glu group, indicating a protective effect of RHC-NE against L-Glu-induced apoptosis.

a) **b)**

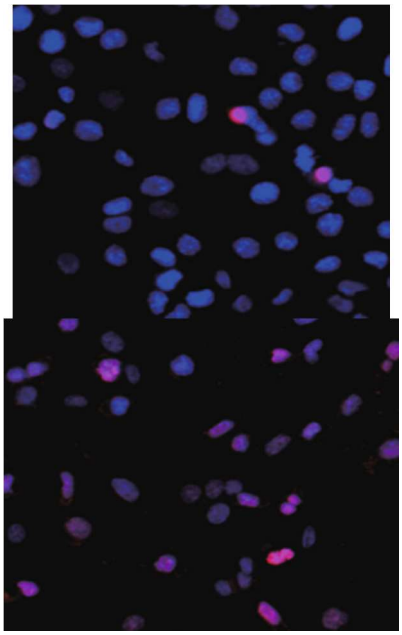

c) d)

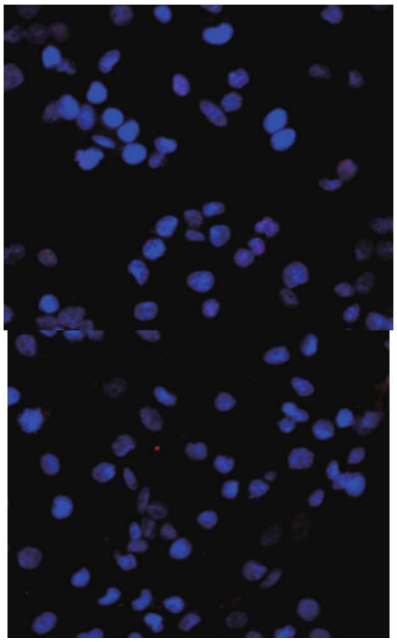

Fig. 7: Effect of RHC-NE on L-Glu-induced apoptosis in SH-SY5Y cells by TUNEL staining: (a) control, (b) model (blank nanoemulsion+30 mmol/L L-Glu), (c) RHC-NE (10 µmol/L) +L-Glu (30 mmol/L), (d) RHC-NE (0.1 µmol/L)+L-Glu (30 mmol/L). Red: TUNEL-positive; blue: DAPI, scale bar = 50 µm

Conclusion

This study demonstrates that administering RHC-NE via the nasal route enhances the bioavailability of RHC. Even at a low dose, RHC-NE preserves the Neuroprotective properties of RHC by mitigating oxidative stress, preventing apoptosis, and modulating the cholinergic system. These findings suggest that RHC-NE could serve as a promising alternative for improving RHC's bioavailability in Alzheimer's disease prevention and treatment. The formulation, developed using nanoemulsion technology, effectively targets the brain through nasal delivery. Additionally, RHC-NE exhibits protective effects against L-Glu-induced neurotoxicity and enhances cognitive function in AD mice, likely through its influence on apoptosis, oxidative stress, and cholinergic regulation. This study highlights the potential of RHC-NE as a therapeutic approach for Alzheimer's disease.

References

1. R.G. Dominguez, T.G. Barrera, J. Vitorica, J.L.G. Ariza. Deciphering metabolic abnormalities associated with Alzheimer's disease in the APP/PS1 mouse model using integrated metabolomic approaches. Biochim. 2015; 110:119-128.

2. B.M. Shah, M. Misra, C.J. Shishoo, H. Padh. Nose to brain microemulsion-based drug delivery system of Rivastigmine: formulation and ex-vivo characterization. Drug Deliv. 2015; 22: 918-930.

3. S.A. Joshi, S.S. Chavhan, K.K. Sawant. Rivastigmine-loaded PLGA and PBCA nanoparticles: preparation, optimization, characterization, in-vitro and pharmacodynamic studies. Eur. J. Pharm. Biopharm. 2010; 76:189-199.

4. G.M. Kerbler, J. Fripp, C.C. Rowe, V.L. Villemagne, O. Salvado, S. Rose, E.J. Coulson. Basal forebrain atrophy correlates with amyloid β burden in Alzheimer's disease. NeuroIm. Clin. 2015; 7:105-113.

5. M. Fazil, S. Md, S. Haque, M. Kumar, S. Baboota, J.K. Sahni, J. Ali. Development and evaluation of Rivastigmine loaded chitosan nanoparticles for brain targeting. Eur. J. Pharm. Sci. 2012; 47: 6-15.

6. K. Nagpal, S.K. Singh, D.N. Mishra. Optimization of brain targeted chitosan nanoparticles of Rivastigmine for improved efficacy and safety. Int. J. Biol. Macrol. 2013; 59: 72-83.

7. M.I. Alam, S. Baboota, A. Ahuja, M. Ali, J. Ali, J.K. Sahni, A. Bhatnagar. Pharmacoscintigraphic evaluation of potential of lipid nanocarriers for nose-to-brain delivery of antidepressant drug. Int. J. Pharm. 2014; 470: 99-106.

8. S. Sood, K. Jain, K. Gowthamarajan. Optimization of curcumin nanoemulsion for intranasal delivery using design of experiment and its toxicity assessment. Colloids Surf. B: Biointerfaces. 2014; 113: 330-337.

9. D.J. Mc Clements. Nanoemulsions versus microemulsions: terminology, differences and similarities. Soft Matter. 2012; 8:1719-1729.

10. G. Mustafa, A. Ahuja, A.H. Al Rohaimi, S. Muslim, A.A. Hassan, S. Baboota, J. Ali. Nano-ropinirole for the management of Parkinsonism: blood–brain pharmacokinetics and carrier localization. Expert Rev. Neurother. 2015; 15: 695-710.

11. S.H. Musa, M. Basria, H.R.F. Masoumia, R.A. Karjibana, E.A. Malek, H. Basri, A.F. Shamsuddin. Formulation optimization of palm kernel oil esters nanoemulsion-loaded with chloramphenicol suitable for meningitis treatment. Colloids Surf. B: Biointerfaces. 2013; 112: 113-119.